MEASUREMENTS OF WIND-SHELTER EFFECTS ON AIR INFILTRATION

D.J. Wilson **J.D. Dale**
ASHRAE Member

ABSTRACT

The effect of wind shelter is complicated by the superposition of wind and temperature difference effects on infiltration. Wind pressure coefficients on vertical walls are strongly dependent on wind direction and the presence of nearby buildings. The importance of both wind direction and wind shelter effects are assessed in the present study.

A long-term experimental program was begun in 1982 to measure air infiltration in six unoccupied test houses of identical exterior dimensions, but with varying tightness. More than 14,000 hours of useful air infiltration measurements have been made using a constant concentration SF_6 tracer gas injector system. The six test houses, built in an east-west row on an exposed farm site, shelter each other for east and west winds and are totally exposed for winds from the north and south. For one house, binned data for narrow ranges of indoor-outdoor temperature difference and wind speed are correlated with wind direction to assess shelter effects. The measurements are used to compute wind exposure coefficients for an orifice-flow infiltration model. Only small variations in total infiltration rate and exposure coefficients are observed with varying wind direction. Both the nondirectional effects of temperature-driven infiltration and the influence of the furnace flue are identified as the major causes for the lack of wind shelter effect.

INTRODUCTION

For an isolated building the wind pressure coefficients on the four walls vary strongly with wind direction. The wind tunnel measurements of Sherman and Ashley (1984) show that wind direction can change infiltration rates by a factor of two or more. Nearby buildings and vegetation that shelters the upwind wall will reduce the stagnation pressure on it and lower the rate of wind-driven infiltration. Wind direction and shelter effects should be strongly dependent on the distribution of leakage sites on the upwind walls.

The superposition of stack and wind pressures acts to reduce the effect of wind direction and shelter on the total infiltration rate. This is easy to see by using the power law infiltration-pressure relation

$$Q = C \Delta P^n \qquad (1)$$

D.J. Wilson and J.D. Dale, Department of Mechanical Engineering, University of Alberta, Edmonton, Alberta T6G 2G8

and assuming that wind- and stack-induced pressures superpose by simple addition,

$$Q^{1/n} = Q_s^{1/n} + Q_w^{1/n} \tag{2}$$

where Q_s and Q_w are the flow rates by stack and wind effects alone. Because stack effect is independent of wind direction or shelter, it remains constant when we differentiate Equation 2 to find the effect of a change in the wind-induced component.

$$\frac{\Delta Q}{Q} = \left[\frac{1}{1 + \left(\frac{Q_s}{Q_w}\right)^{1/n}} \right] \frac{\Delta Q_w}{Q_w} \tag{3}$$

When wind and stack effects are equal, $Q_s = Q_w$, Equation 3 shows that a 10% change in Q_w will only cause a 5% change in total infiltration. In cold climates, where stack flow, Q_s, is often greater than Q_w, the total infiltration is quite insensitive to wind effect. For example, using $n = 0.65$ and $Q_s = 2\ Q_w$, a 10% change in Q_w produces only a 2.5% change in total Q.

TEST FACILITY

The Alberta Home Heating Research Facility consists of six unoccupied test houses that have been continuously monitored since 1981 for building component energy losses and air infiltration rates. The units allow side-by-side testing to reduce the effects of weather variability in conducting studies of various energy conservation and ventilation strategies.

The present study uses infiltration data taken during the fall, winter and spring heating seasons in test house 5, located with one house on its east side and a row of four houses to the west. This house was chosen because it represents typical 1970's Canadian wood frame construction. Data from four heating seasons, 1981 to 1985 were pooled to provide a large data base.

The six test units are one-room single-story modules built to residential wood frame construction standards. The floor area is about half the size of a typical bungalow, with a house 5. The locations of the major leakage sites are shown in the schematic in Figure 1. For clarity, the overhanging roof eaves are not shown on the figure. The air-vapor barrier is penetrated by eight electrical outlet boxes on the inside walls and three electrical boxes in the ceiling.

To simulate operation of a forced-air furnace, a ducted electrical heater is located in the basement, with a centrifugal fan distributing air through under-floor ducts. To promote mixing and prevent stratification, air intakes are located near the basement floor and basement ceiling, and the heated air discharged to the single upper room returns to the basement through a large open stairwell. The fan is operated continuously, and inside temperature is controlled with a standard room thermostat set to a constant value of about 22°C.

Five of the six units, including the one discussed in the present study, are provided with a standard Class B natural gas furnace vent, which acts as the major exfiltration site. This unheated vent begins about 2 meters above the basement floor and passes through the upper level floor, ceiling, and roof to terminate in a rain cap above the roof peak. Because the unheated flue is continuously filled with room temperature air, it is equivalent to a leakage with the same flow resistance located at a height above the ceiling equal to the distance from ceiling to rain cap.

TERRAIN AND WIND MEASUREMENT

The test houses are located on the University of Alberta Agricultural Research Farm about 10 km south of the city of Edmonton at 53.5°N latitude. They are situated in a closely spaced east-west line with about 2.8 m separation between their side walls. False end walls with a height of 3.0 m, but without roof gable peaks, were constructed beside the end houses of the line to provide them with equivalent wind shelter and solar shading.

The flat exposed site stands on rural farmland, whose fields are planted in forage and cereal crops in summer, with snow-covered stubble in winter. Windbreaks of deciduous trees cross the landscape at intervals of a few kilometers, with one such windbreak located about 250 m to the north of the line of houses. The houses are totally exposed to south and east winds, with a few single-story farm buildings located about 50 to 100 m to the west providing some shelter for winds from the west to northwest direction.

Micrometerological towers are located midway along the row of houses on both the north and south sides of the house line. The wind speed at a 10 m height is measured with low-friction cup anemometers and vanes on both towers, with the data acquisition system recording the value from the tower upwind of the houses. However, there was usually little difference in the 10 m windspeeds, so that the two-tower system simply provided an additional measure of reliability.

Because the anemometers are located close to the houses, they have the same wind exposure, although at a somewhat greater height above ground. This means that it is not necessary to account explicitly for nearby buildings and windbreaks. One exception to this is the influence of a large solar collector panel located a few meters from the south wall of unit 6. This provides some wind shelter for ESE winds on unit 5, the test house in the present study. We will later see that this shelter effect (and in fact all shelter effect) is negligible.

INFILTRATION MEASUREMENTS

Continuous infiltration measurements were carried out in the six test houses using a constant concentration SF_6 tracer gas injection system in each house. Two independent infrared analyzers each sample three houses in sequence through a manifold controlled by solenoid valves.

A microcomputer data acquisition system monitoring the analyzers was used to control the discrete injections of tracer gas required to maintain the concentration at a constant level of 5 ppm. The sampling system monitored each of the houses for 2.5 minutes, with a return period of 7.5 minutes to give 8 infiltration pulse counts per hour. This 7.5 minute return period allowed ample time for the previous series of injections to mix completely within the house volume and to allow the necessary time for the infrared analyzer to draw a sample from an adjacent house. By monitoring and reinjecting tracer gas eight times per hour, the building concentration was maintained within 0.2 ppm of the nominal 5 ppm setpoint. Hourly averages of the tracer gas injection rate, and wind speed and direction, were recorded.

An earlier version of this system is described by Wilson and Pittman (1983). The only significant modifications to the system have been the use of a smaller injector volume to increase injection count resolution and an automatic zeroing check carried out daily by sampling outside air through a line located on the south meteorological tower. In addition to the daily zero concentration checks, the detector was calibrated at monthly intervals using a closed-loop system with syringe injection of SF_6 mixtures.

An error analysis of the injection and concentration measuring systems predicted that the standard deviation in infiltration rate was ± 2.5% of Q added to an absolute error of ± 0.5 m^3/h. For the infiltration measurements in unit 5 this is about a ± 4% total standard deviation in Q or ± 8% to encompass 95% of the data. It will be seen later that this experimental error accounts for about one-third to one-half of the observed data scatter.

ORIFICE FLOW INFILTRATION MODEL

To help generalize experimental results for the particular house considered, it is useful to use the data to calculate wind coefficients in an infiltration model, to provide a simple way of normalizing the measured data. The most widely used predictive model is Sherman's (1980) orifice flow approximation, which assumes that the exponent in Equation 1 is n=0.5. For a particular house, the actual flow coefficient, C, and exponent, n, are used to calculate the equivalent orifice flow leakage area, L, at some reference pressure. For test house 5 the coefficients C and n in Equation 1 and the leakage area L are given in Table 1. The orifice flow air infiltration model developed by Sherman (1980) has recently been summarized in Sherman and Modera (1984). The separate wind induced and stack flow rates are given by

$$Q_w = L(P_w U^2)^{0.5} \tag{4}$$

$$Q_s = L(P_s \Delta T)^{0.5} \tag{5}$$

The coefficients are calculated from

$$P_w = \left[C'(1-R_o)^{1/3} \frac{U_c}{U}\right]^2 \tag{6}$$

$$P_s = \frac{gH_s}{T_i}\left[\frac{1 + 0.5R}{3}\right]^2\left[1 - \left[\frac{X}{2-R}\right]^2\right]^3 \tag{7}$$

where C', the wind shielding coefficient, is the parameter of interest.

It is important to recognize that the furnace flue leakage area, L_{flue}, contributes to the stack coefficient, P_s, as a hole in the ceiling but is not sheltered from the wind like other ceiling leaks. To account for this difference, Sherman's model has been modified to use different horizontal to wall leakage ratios, R_o, and R, in the wind and stack coefficients. These are defined in terms of the leakage areas of the floor L_f, the ceiling (including flue), L_c, and the flue alone, L

$$R = \frac{L_c + L_f}{L} \tag{8}$$

$$R_o = R - \frac{L_{flue}}{L} \tag{9}$$

$$X = \frac{L_c - L_f}{L} \tag{10}$$

Estimating the "floor" leakage area, L_f, for a house with a basement is more a matter of guesswork than science. Starting with the premise that some of the leakage sites on the lower part of the foundation might be well enough sheltered from the wind to act like horizontal floor leaks, it was estimated that 17% of the total leakage acts like an effective floor, L_f. The distribution of leakage sites shown in Figure 1 shows that at best such an assumption is plausible speculation.

Using the total and flue leakage areas, L and L_{flue} from Table 1, along with the assumption that $L_f = 0.17L$ yields values of X = 0.49, R = 0.83, and R_o = 0.25. With these in in Equation 7, assuming a distance H_s = 9.2 ft (2.8 m) between the highest and lowest leakage sites and T_i = 531°R (295°K), the stack coefficient is $P_s = 0.012\ m^2 s^{-2} °C^{-1}$.

The wind speed at U_c ceiling height, 9.8 ft (3 m) above ground, was calculated to be 83% of the speed U on the nearby instrument tower at 33 ft (10 m), using an assumed power law velocity profile varying as height to the exponent 0.155. With this, the wind coefficient in Equation 6 is

$$P_w = (0.75C')^2 \tag{11}$$

Using the argument that it is possible to add the separate wind and stack pressures, Sherman's orifice flow model superposes the wind- and stack-induced flows to produce a total flow, Q, of

$$Q = (Q_s^2 + Q_w^2)^{0.5} \tag{12}$$

CALCULATING WIND SHIELDING COEFFICIENTS

The wind shielding coefficient, C', in Sherman's model was calculated from Equations 4, 6, and 11, using Equation 12 to correct for stack effect. Combining these equations yields

$$C' = 1.33 \left[\left(\frac{Q}{UL}\right)^2 - P_s \frac{\Delta T}{U^2} \right]^{0.5} \tag{13}$$

Using this, measured shielding coefficients were computed from binned data sets over U and ΔT selected from the 14,000 hours of available data. A value of P_s = 0.01 was used in the temperature correction term, $P_s \Delta T/U^2$. Average values over all wind directions were calculated by first averaging over 5° direction increments and then taking the mean of the resulting 72 values to find the 360° average. This procedure removed any bias that might be present due to prevailing wind directions increasing the number of data points for one direction. The magnitude of the stack effect correction term in Equation 13 was determined by setting P_s = 0 and computing the uncorrected wind exposure factor

$$C'_{uncorrected} = 1.33 \left[\frac{Q}{UL}\right] \tag{14}$$

FIELD MEASUREMENT RESULTS

To provide a high degree of resolution, it is desirable to choose narrow ranges of wind speed and temperature for the binned data sets, which can then be plotted against wind angle. In practice, even with 14,000 hours of data, it was difficult to maintain an adequate sample size when extremes of speed or temperature difference were chosen. A compromise was required in which wind speed and temperature were limited to frequently occurring values.

The data in Figure 2 are an example of one such set in which the stack effect provides the largest contribution to the infiltration pressure difference. Because stack effects are independent of wind direction, the flow rate, Q, shows the expected constant value with wind angle. The lines drawn on the polar plots are smoothed by first averaging the data in 5°

sectors and then smoothing the curve by averaging over a 25° sector (two 5° sectors on each side of the specified angle).

When the flow rate is normalized by wind speed to form Q/U, the data scatter in Figure 2 increases. This is expected, because the wind and stack contributions to the total flow are about equal for this data set. When normalized by U, the stack component varies like Q_s/U. and the variation of U from 1.0 to 2.0 m/s accounts for the increased scatter.

The wind shelter coefficient in Figure 2 does not indicate any significant shelter effects of nearby houses for east or west winds. The data in Figure 3 for a higher wind speed and the same temperature range for Figure 2 also shows no significant directional dependence of flow rate or shielding coefficient, C'. The shielding of the test house varies from an open rural exposure for north and south winds to highly sheltered by nearby buildings for east and west winds, so this lack of wind direction dependence was totally unexpected.

Why is there no wind shelter from the adjacent houses? We will see later that the probable cause of this insensitivity is the influence of the furnace flue. The rain cap on this flue extends above the roof into a low pressure region, which has a pressure coefficient that is relatively insensitive to wind direction. Because the furnace flue contributes 57% of the total leakage area, its lack of wind direction sensitivity is the dominant factor.

In both Figures 2 and 3, the angular variation of wind speed is plotted using a 25° smoothing band through the averages of each of the 5° sectors. Even with a sample size of 600 hourly averages and a relatively narrow range of wind speeds, there is still some bias in average speed with wind direction. Fortunately the variation is small, and its effect on the total flow, Q, is probably insignificant.

Another feature of Figures 2 and 3 is the increased data scatter that occurs for winds from the southeast. One reason for this is that southeast winds occur much more frequently than winds from other directions, and the larger number of data points increases the probability of observing extreme values. Overprinting of symbols from the large sample size of 500-600 hours makes it difficult for the reader to see the distribution of sample size with wind angle. In fact, the 5° segment bins for southeast winds typically contain two to three times as many points as those for other directions. Another possible, but less likely, explanation is that wind shelter from the solar collector panel located to the southeast of house 5 may have produced turbulence and influenced the infiltration variability.

In Figure 4, a wide range of wind speeds and a small temperature difference were chosen to produce a large sample size dominated by wind-induced flow. This set should give the best estimate for wind shielding coefficients by minimizing the stack effect correction term in Equation 13. In fact, these coefficients are much lower and vary differently with wind direction than those observed for lower windspeeds and higher temperature differences. The uncorrected shielding coefficients, which are proportional to Q/U, and the corrected value C', both show a strong variation with wind direction. However, this variation is strongly correlated with the wind speed bias that occurs for this large range from 2 to 20 m/s.

In theory, the shielding coefficient should be independent of wind speed if orifice flow is a good approximation. When Q follows the power law in Equation 1, it is easy to show, using $\Delta P \propto U^2$ in Equation 1 and combining this with Equation 14, that

$$C' \propto U^{2n-1} \qquad (15)$$

For the test house, n = 0.6 is a good estimate (see Table 1). This value implies that $C' \propto U^{0.2}$. In Figure 4, the high degree correlation of C' with U suggested values of n ranging from 0.7 to 1.4, much larger than expected. In any case, a comparison of the wind direction dependence of shielding coefficient and of average wind speed shows that most of the variation in shielding coefficient can be assigned to its wind speed dependence rather than any actual directional or shielding effects.

What is even more disconcerting is that the average shielding coefficient shows a strong dependence on the stack pressure to wind pressure ratio, which is proportional to $\Delta T/U^2$. This dependence is evident in Table 2 where the average shielding coefficient, $\overline{C'}$, varies by more than a factor of 2 as we move from the stack dominated to the wind dominated regime. This variation suggests that the stack effect correction in Equation 13 was too small. However, increasing P_s from 0.01 to 0.025 did not significantly change the variation and resulted in a large number of negative values for the measured corrected shielding coefficient. From this we concluded that an orifice flow infiltration model with sum of squares superposition of stack and wind flows may not be an adequate representation of the infiltration processes for the test houses. Because the measured fan pressurization exponent was about n = 0.6, it may be the stack and wind superposition that is at fault, rather than the orifice flow model, which uses n=0.5.

CALCULATING LEAKAGE AREA DISTRIBUTION EFFECTS

It is difficult to determine experimentally whether the observed lack of wind direction and shielding effects is the norm, or whether it is an anomaly caused by the particular leakage distribution on the test house. To investigate this, building surface pressure coefficients were estimated from wind tunnel measurements of other investigators and used to compute the effect of leakage area distribution.

Sherman (1980) predicted the wind shielding coefficient using averaged wind tunnel pressure measurements by Akins, Peturka, and Cermak (1979). For each wind direction these surface pressure coefficients were used to estimate the internal building pressure for a uniform distribution of leakage area. The internal pressure coefficients were then used with Sherman's (1980) orifice flow model to compute the shielding coefficient, C', for several wind directions. These C' values were then integrated with wind angle to determine the 360° average, $\overline{C'}$. The results of these calculations are shown in Figure 5, where it is apparent that the presence of a furnace flue with 50% of the total leakage area can virtually eliminate the directional dependence of C'.

The shielding coefficients in Figure 5 are for an isolated building. The question still remains as to why the adjacent buildings on the east and west sides failed to provide wind shelter. Again, the explanation appears to be related to the influence of the furnace flue, which protrudes above the roof into a region where the pressure is insensitive to the presence of nearby buildings of the same height.

CONCLUSION

The present study used a large data base of over 14,000 hours of infiltration data on a single house to examine the effects of wind direction and shelter from adjacent buildings. The measurements and calculations indicate that:

1. A furnace flue that terminates above the roof, and which makes up about half the leakage area, will remove any wind direction dependence of wind induced

infiltration. The flue is also the most likely reason why the adjacent houses (of the same height) failed to provide any significant shielding.

2. Where stack-induced infiltration caused by temperature differences is dominant, this nondirectional effect will strongly reduce the influence of wind shelter.
3. The wind shielding coefficient C' in the orifice flow model exhibits an unrealistically strong dependence on wind speed. The use of a power law with n larger than 0.5 reduces, but does not eliminate, the wind speed dependence.
4. The large observed variation of shielding coefficient, which occurs with changes in the ratio of stack to wind pressures (see Table 2), suggests that a direct sum-of-squares superposition of wind and stack flow rates in Equation (12) may not be appropriate.

These conclusions, taken together, indicate that accounting for wind direction and shelter effects is less important than the need to make improvements in air infiltration models where the furnace flue makes an important contribution to total leakage area. It may be useful to develop a separate model for flue flow that can be superposed on a general infiltration calculation for uniformly distributed leakage sites. Lumping the furnace flue with other leakage areas may cause excessive error in the simple orifice flow model.

NOMENCLATURE

C = flow coefficient in Equation 1, $m^3/s\ (Pa)^n$
C' = wind shielding coefficient
$\overline{C}'$ = wind shielding coefficient averaged overall wind directions (360° average)
L = total leakage area at a specified reference pressure, m^2
L_c = leakage area in ceiling, including flue, m^2
L_f = leakage area of furnace flue, m^2
L_{flue} = leakage area of furnace flue, m^2
n = flow exponent in Equation 1
P_s = stack coefficient, $m^2/s^2°C$
P_w = wind coefficient
Q = combined infiltration rate from both stack and wind effects, m^3/s
Q_s = infiltration rate induced by indoor-outdoor temperature difference in the absence of wind, m^3/s
Q_w = infiltration rate induced by wind in the absence of indoor-outdoor temperature difference, m^3/s
R_o = ratio of horizontal sheltered (ceiling and floor) leakage area to total leakage area
R = ratio of horizontal sheltered and unsheltered leakage are to total leakage area
T_i = indoor temperature, °K
U = wind speed at instrument height on local meteorological tower, m/s
U_c = wind speed at building ceiling height, m/s
X = ratio of difference between ceiling and floor leakage area to total leakage area
ΔT = indoor-outdoor temperature difference, °C
θ = wind direction measured from north in easterly direction (N=0°, E=90°, S=180°, W=270°)

REFERENCES

Akins, R.E.; Peturka, J.A.; and Cermak, J.E. 1979, "Averaged pressure coefficients for rectangular buildings." Proceedings Fifth International Conference on Wind Engineering, Fort Collins, Colorado, July 1979, pp. 369-380.

Sherman, M.H. 1980. "Air infiltration in buildings." Ph.D. thesis, University of California, Berkeley, pp. 173-188 (also Lawrence Berkeley Laboratory Report LBL-10712).

Sherman, M., and Ashley, S. 1984. "The calculation of natural ventilation and comfort." ASHRAE Transactions 90 part 1, pp. (also Lawrence Berkeley Laboratory Report LBL-16036).

Sherman, M.H., and Modera, M.P. 1984. "Comparison of measured and predicted infiltration using the LBL infiltration model." Proceedings ASTM Symposium on Measured Air Leakage Performance of Buildings, Philadelphia, April 1984 (also Lawrence Berkeley Laboratory Report LBL-17001).

Wilson, D.J., and Pittman, W. 1983. "Correlating measured infiltration for wind from a single direction." ASHRAE Transactions 89:2, pp. 211-227.

ACKNOWLEDGMENTS

The experiments and data analysis were supported through strategic and operating grants from the Natural Sciences and Engineering Research Council of Canada and from the Department of Energy Mines and Natural Resources.

TABLE 1

Dimensions and Leakage Characteristics
Test House 5

Walls, N and S	24 ft (7.32 m) outside 23.3 ft (7.11 m) inside
Walls, E and W	22 ft (6.71 m) outside 21.3 ft (6.50 m) inside
Inside Wall Height	8 ft (2.44 m)
Basement Wall Height (incl. 0.26 m floor joists)	2 ft (0.61 m) above grade 6.8 ft (2.07 m) below grade
Door Orifice Area	19.6 ft^2 (1.82 m^2)
Plan Area (outside)	528 ft^2 (49.1 m^2)
Floor Area (inside)	496 ft^2 (46.2 m^2)
Envelope Area (above grade)	1,884 ft^2 (175 m^2)
$\frac{\text{Ceiling Area}}{\text{Envelope Area}}$	0.264
$\frac{\text{Window Area}}{\text{Plan Area}}$	0.10
Internal Air Volume	7769 ft^3 (220 m^3)
Pressurization Leakage ΔP in Pascals	$Q = 0.021\ (\Delta P)^{0.56}$ m^3/s
Depressurization leakage ΔP in Pascals	$Q = 0.014\ (\Delta P)^{0.62}$ m^3/s
Total Leakage Area, L press-depress avg at 4 Pa	0.157 ft^2 (0.0146 m^2)
Flue Leakage Area press-depress avg at 4 Pa	0.0904 ft^2 (0.0084 m^2)

TABLE 2

Direction Averaged Wind Exposure Coefficients

RANGE		$\frac{\overline{\Delta T}}{\overline{U}^2}$	$\overline{U}$	$\overline{C'}$	$\overline{C'}$ uncorrected for ΔT
U m/s	ΔT °C	°Cs/m	m/s		
1-2	20-25°	10.0	1.52	0.650	0.780
2-3	20-25°	3.6	2.50	0.472	0.536
1-10	0-5°	0.21	3.45	0.245	0.266
2-20	0-5°	0.16	3.93	0.261	0.271

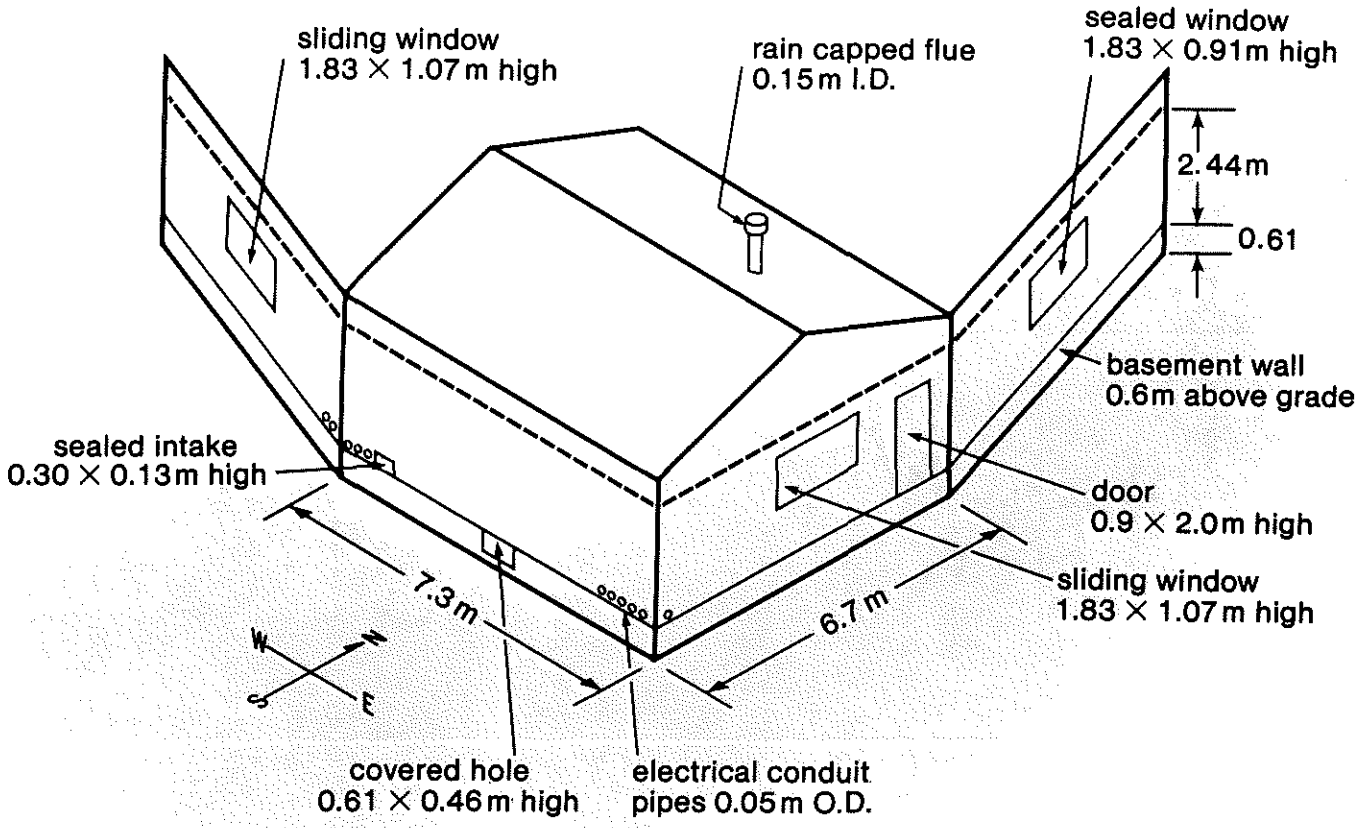

Figure 1. Infiltration leakage sites on test house 5

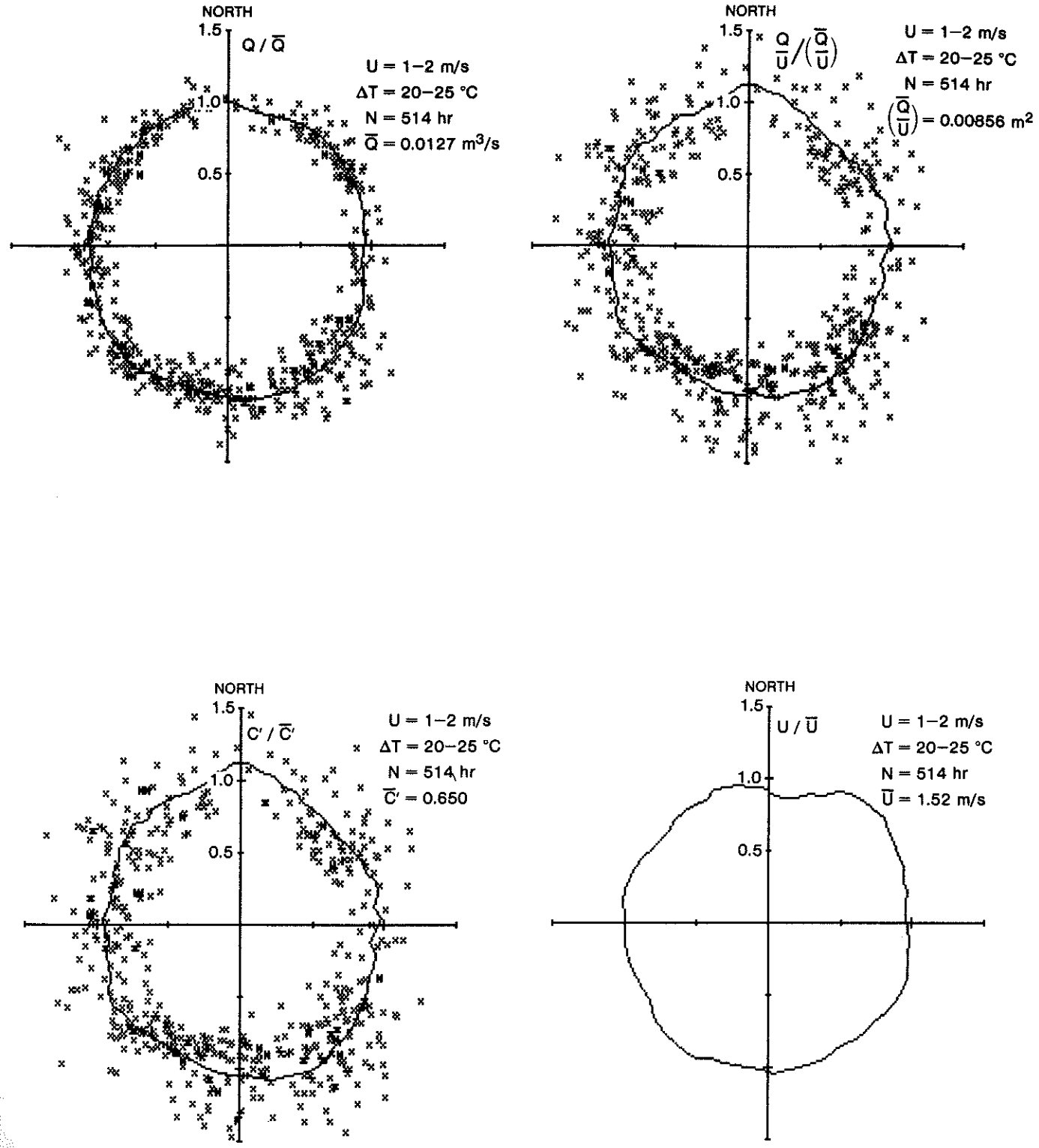

Figure 2. Measured effect of wind direction on infiltration when stack effect is dominant

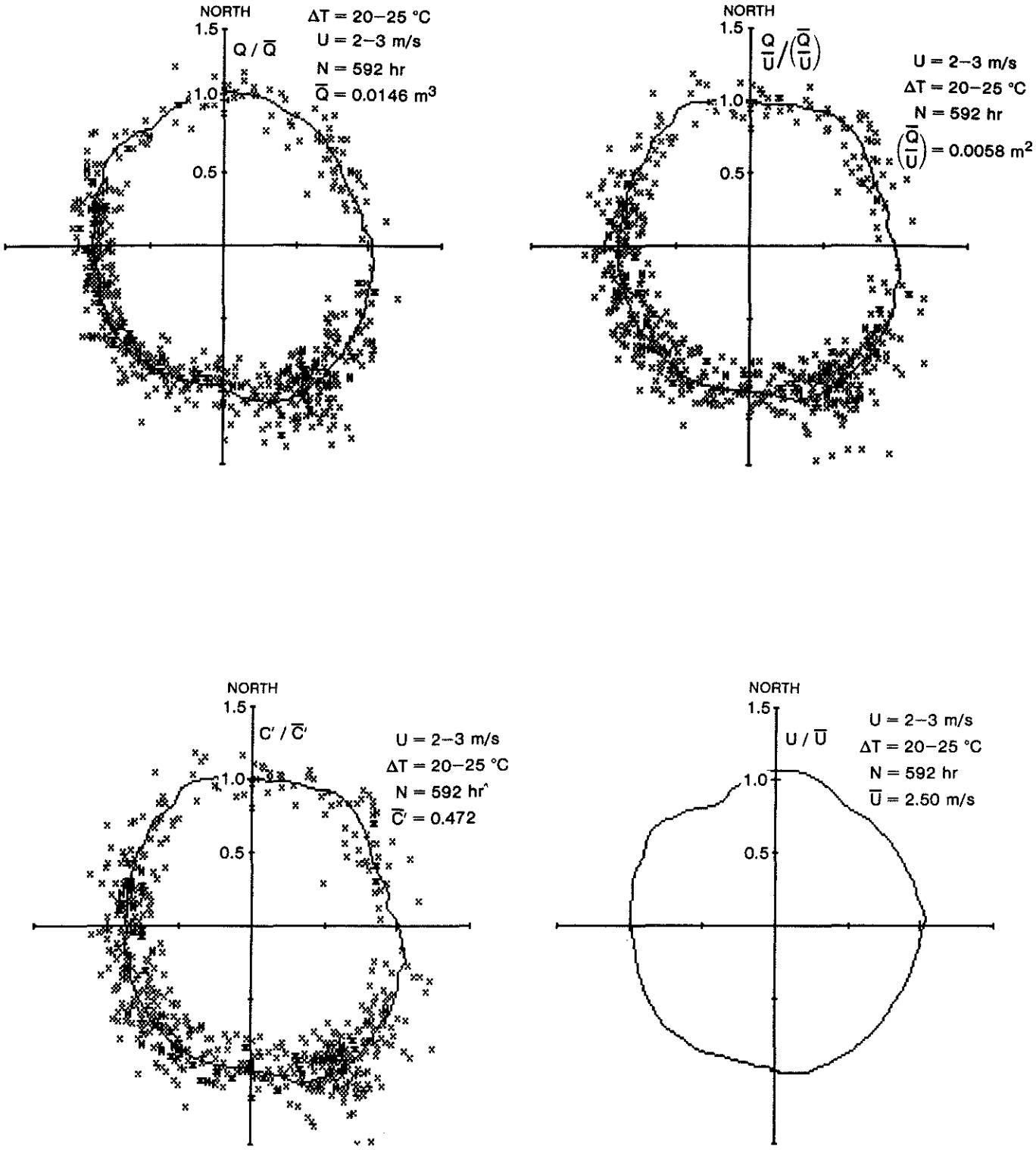

Figure 3. Measured effect of wind direction on infiltration when wind and stack effects are of similar size

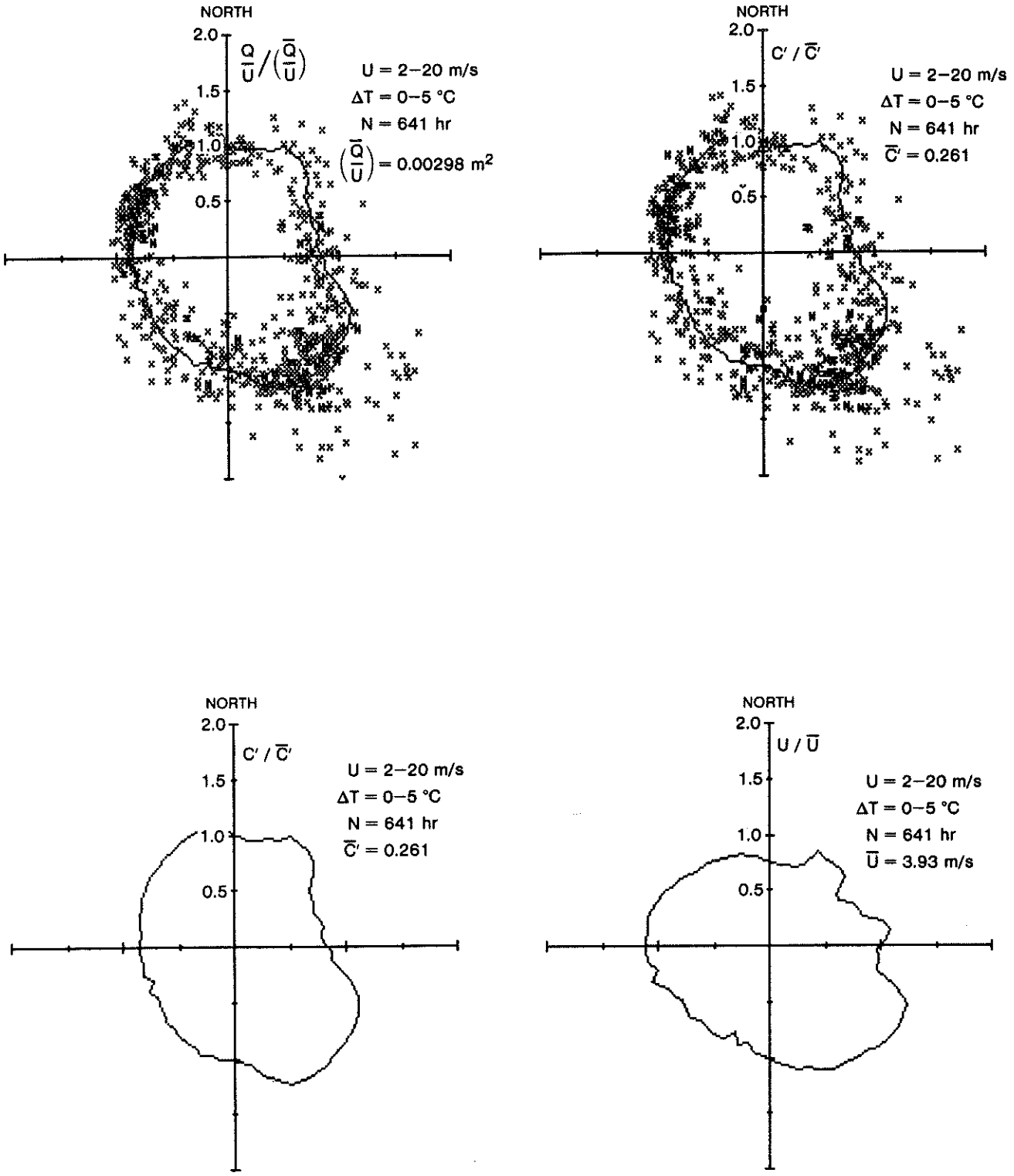

Figure 4. Measured effect of wind direction on infiltration when wind effect is dominant

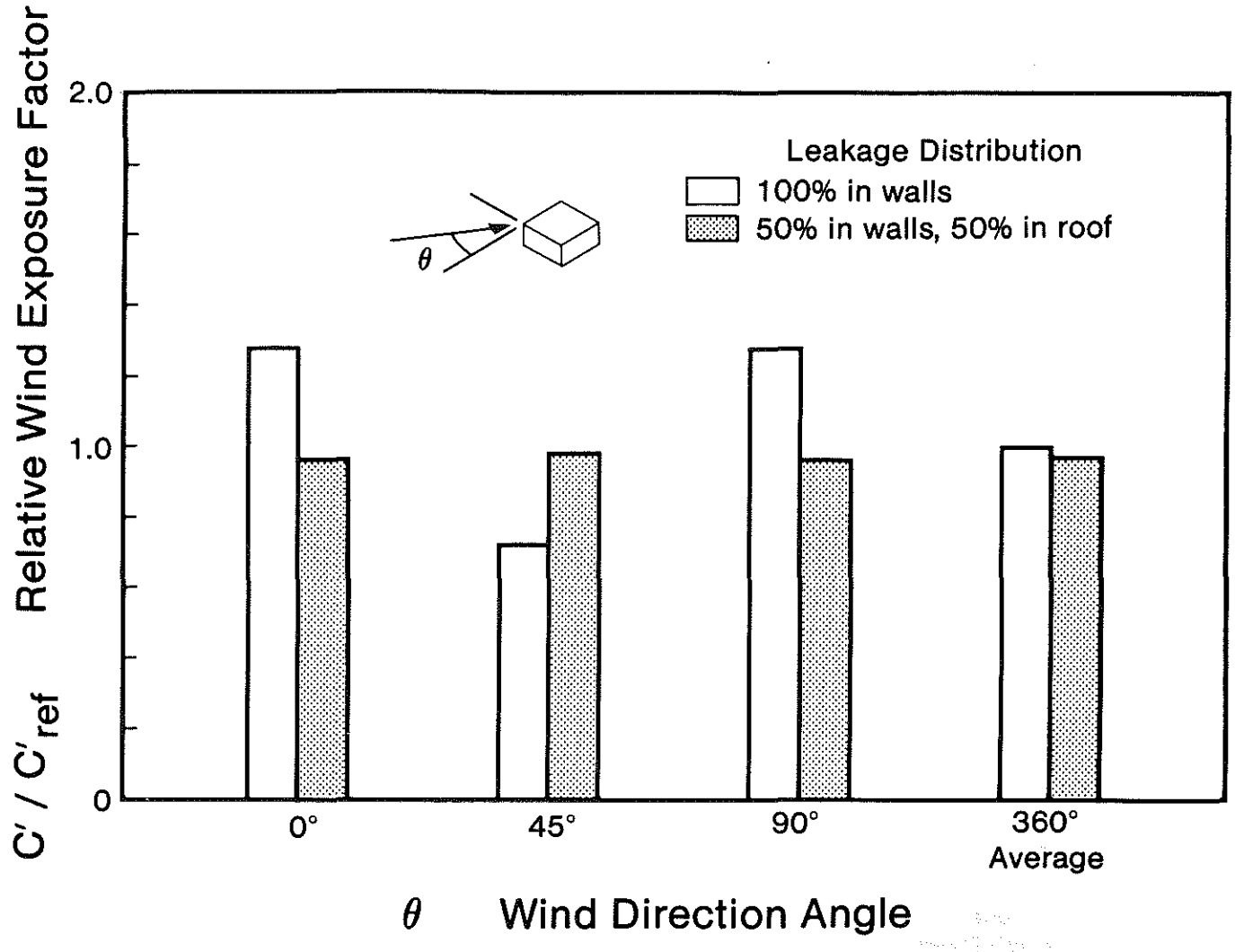

Figure 5. Calculated effect of leakage distribution on wind shielding coefficients for an isolated flat-roofed building using pressure coefficients from Aikens, Peturka, and Cermak (1979). Reference shielding coefficient is a 360° average with all leaks in walls